Analysis the vortex ring state and propeller state of floating offshore wind turbines and verification of their prediction criteria by comparing with a CFD model

Dong, Jing; Viré, Axelle; Li, Zhangrui

DOI
10.1016/j.renene.2021.11.053

Publication date
2022

Document Version
Final published version

Published in
Renewable Energy

Renewable Energy 184 (2022) 15–25

Contents lists available at ScienceDirect

Renewable Energy

journal homepage: www.elsevier.com/locate/renene

Analysis the vortex ring state and propeller state of floating offshore wind turbines and verification of their prediction criteria by comparing with a CFD model

Jing Dong [a, b, *], Axelle Viré [a], Zhangrui Li [c]

[a] Delft University of Technology, Wind Energy Section, Kluyverweg 1, 2629 HS, Delft, the Netherlands
[b] School of Naval Architecture and Ocean Engineering, Jiangsu University of Science and Technology, Zhenjiang, 212003, China
[c] Wind Energy Group, Shanghai Electric, Shanghai, China

ARTICLE INFO

Article history:
Received 21 June 2021
Received in revised form
26 October 2021
Accepted 13 November 2021
Available online 24 November 2021

Keywords:
Vortex ring state (VRS)
Propeller state
Floating offshore wind turbine (FOWT)
Free wake vortex method
Wind energy
Aerodynamics

ABSTRACT

In our previous study, the vortex ring state (VRS) prediction criteria were introduced from helicopter's realm and applied to floating offshore wind turbines (FOWTs). The existence of the VRS on FOWTs was also successfully predicted. However, the prediction criteria we used have not been verified by comparing them with similar studies because of the lack of reference publications — until recently. In this paper, a comparative analysis of the VRS phenomenon of an FOWT is done and aerodynamic performance of the FOWT is evaluated. We compare the VRS results predicted based on the criteria we proposed with a new study about the VRS by means of a computational fluid dynamics (CFD) method. The aerodynamic performance of an FOWT undergoing surge motions is simulated with an in-house code based on a free wake vortex method. Similarities and differences of the two studies are compared and discussed. The propeller state of the rotor is further analyzed to gain a deeper understanding of the working state change of FOWTs as well as to strengthen the research in this area.

1. Introduction

Floating offshore wind turbines (FOWTs) are more flexible than bottom-fixed ones, and therefore can experience larger unsteady loads during their operation. According to different levels of blade-wake interaction, there are four working states of a rotor: windmill state, turbulence state, vortex ring state, and propeller state as shown Fig. 1, where the blue arrow represents the direction of the streamlines and the yellow arrows represent the direction of the rotor motion. During the windmill state, the rotor extracts energy from the flow to rotate and the streamlines extend and expand orderly in the wake. During the turbulent state, the rotor also extracts energy from the flow, but the streamlines becomes chaotic in the wake. The vortex ring state (VRS), or 'settling with power', occurs when the rotor of the FOWT moves downwind, which leads to the accumulation of the vortices in the wake and form a loop around the rotor. The propeller state is onset when the flow reversal occurs all through the rotor and the wind turbine outputs energy into the flow like a propeller. In Fig. 2 [1], the four wind turbine rotor working states corresponding to axial induction factor a are illustrated. From the figure it can be seen that when $0 < a < 0.5$, the rotor is in windmill working state; when $0.5 < a < 1.0$, the rotor is in turbulence state and when $a > 1.0$, the rotor is in propeller state. In particular, the vortex ring state does not explicitly occupy any phase along the axis of a. It is considered to be exist in a stage when a is close to 1. In this paper, we particularly research on the vortex ring state of floating offshore wind turbines.

Different working states are researched on at different stage of the development of wind turbine technology. The windmill and turbulent working states are the most relevant states for wind turbines installed onshore and on fixed foundations offshore. Because the vortex ring state rarely occurs for bottom-fixed turbines, it has not been widely research on for wind turbines yet. However, the fact that FOWTs experience much larger rotor motions than their bottom-fixed counterpart led by floating platforms objectively provides the environmental condition for the occurrence of the VRS on FOWTs. From the literature of helicopters, we know that the vortex ring state is characterised as [2] [[,][3]]: (i) The rotation becomes apparently unsteady and aperiodic. (ii) The

* Corresponding author. Delft University of Technology, Wind Energy Section, Kluyverweg 1, 2629 HS, Delft, the Netherlands.
E-mail addresses: j.dong-2@tudelft.nl, dj0116@163.com (J. Dong).

https://doi.org/10.1016/j.renene.2021.11.053
0960-1481/

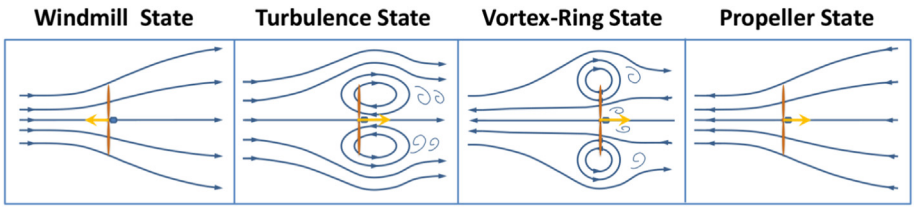

Fig. 1. Four working states of FOWTs (adapted from Ref. [4]).

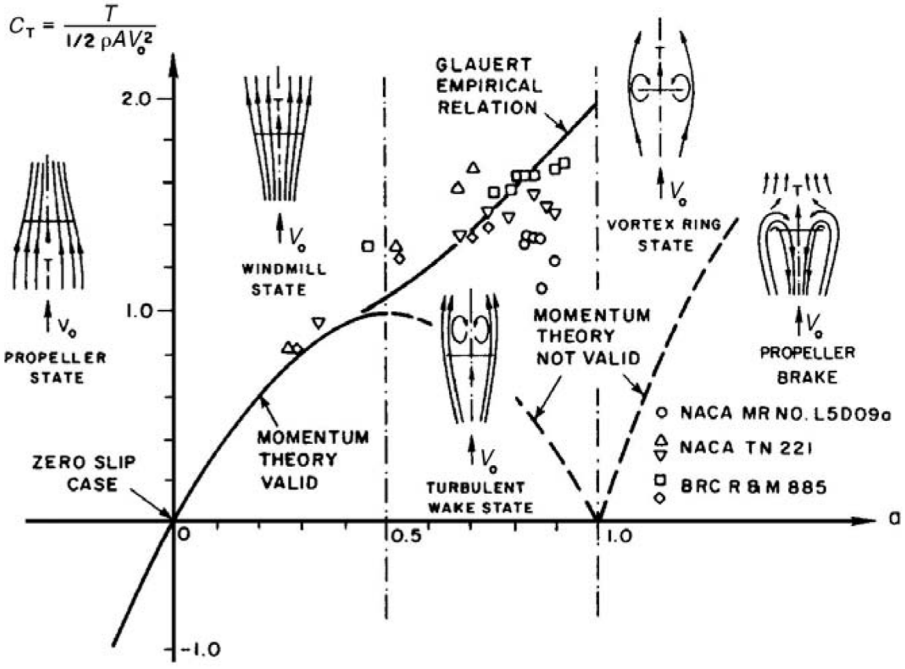

Fig. 2. The rotor working states corresponding to axial induction factor a (taken from Ref. [1]).

blades experience successive forward and backward velocities, which can lead to significant blade flapping and a loss of rotor control. (iii) The level of thrust fluctuations is high, which threatens the landing safety the flight control of the aircraft. Accordingly, with increasing development of floating offshore wind energy, the phenomenon of the VRS of FOWTs is worth to be researched on.

Aerodynamic problems of a wind turbine about all the working states as introduced above can be considered as rotor-wake interaction problems. So far, studies about rotor-wake interaction problems for floating wind turbines are mostly based on platform motions. Sebastian researched on the unsteady aerodynamic characteristics of FOWTs by means of BEM method and coupled analysis and hypothesized [5] that the VRS occurs on FOWTs as a transient phenomenon. Tran [6,7] studied the unsteady aerodynamics of the FOWT platform motion using a computational fluid dynamics (CFD) model. Jeon [8] studied the unsteady aerodynamics of FOWTs in platform pitching motion using the vortex lattice method. Kyle [9] researched on the alleviation of the vortex ring state of FOWTs using a modified blade-tip shape based on a CFD method. Also, Kyle [10] simulated the surge motion of FOWTs with rated and below rated wind speeds with CFD model. The propeller and vortex ring state were identified during the rotor motion, where the VRS was observed with blade tip-vortex interaction and root vortex recirculation with a negative relative rotor velocity.

In helicopter's realm, different criteria for the VRS prediction were developed based on momentum theory, field test, experiments, numerical simulation and so on. Different criteria can predict different range of the VRS boundaries [11]. In our earlier studies [4,12], we simulated the six-degree of freedom coupled motions of FOWTs with both regular and irregular wave conditions with a set of different wind speeds, and we quantitatively predict the VRS boundaries of FOWTs with the axial induction factor as well as two different VRS prediction criteria adapted from the research on helicopter VRS— Wolkovitch's criterion [13] and Peters' criterion [14]. The axial induction factor $a = 1$ is the border of the turbulent state and the propeller state, where the vortex ring state should be exist [1]. Wolkovitch's criterion is considered to predict the center of the vortex ring state, while Peters' criterion predicts the boundaries of the vortex ring state [14].

In order to simulate of the vortex ring state and more general rotor-wake interaction problems of FOWTs, the platform motion, structural dynamics and aerodynamics of the rotor need to be considered simultaneously, which depends on the hydro-aero-elastic coupled analysis. Because the coupled analysis needs fit together different modules, lower fidelity algorithms are often adopt to offset the time cost from large number of computations. So far, the coupled analysis tools for floating offshore wind turbines are almost exclusively based on the blade element momentum (BEM) theory, whose applicability to unsteady rotor-wake interactions is limited. Aside from BEM, various vortex based methods have been developed and applied to the aerodynamic

calculation of wind turbine rotors under motion. For example, the wake structure of FOWTs has been represented by vortex filaments such as the free wake vortex filament (FWVF) method of Sebastian [15], vortex particles such as the nonlinear vortex lattice method (NVLM) of Lee [16], and free wake vortex ring (FWVR) models developed by Afjeh [17], de Vaal [18] and Dong [19].

Form the literature, it is quite interesting to see that Kyle et al. [10] researched on the same topic with us, while with a different wind turbine simulation method and identified the VRS in a way mainly based on observation. In this paper, we reproduced the load cases of Kyle [10] with our in-house code of a free wake vortex ring methods [19], predicted the VRS boundary with criteria given in our previous research [4] and compared the results with Kyle's paper. For the convenience of expression, the paper of Kyle et al. [10] is described as 'the literature' in the following parts of this paper unless otherwise defined.

The aim of this paper is two fold, firstly, we would like to verify the criteria we applied for the prediction of the VRS of FOWTs; secondly, we would also like to gain a deeper understanding of the VRS phenomenon of FOWTs as well as to strengthen the research in this area. This paper is organized as follows: in Section 2 the aerodynamic model based on a free wake vortex ring method is introduced; in Section 3 the 5 MW wind turbine and coordinate systems used for the simulation are introduced; in Section 4 two criteria for the VRS prediction that are applied in this paper are given; in Section 5 environmental conditions and rotor motions are described; in Section 6 research methods are compared with the literature; and in Section 7 the prediction results are analyzed and they are systematically compared; Section 8 is the conclusion of this research.

2. Aerodynamics model of the rotor

A free wake vortex ring method [19] is used to build up an aerodynamic model of the rotor to simulate the rotor-wake interaction. The fluid model and the blade model of the aerodynamic model are introduced as below.

2.1. Fluid model

The fluid model consists of two parts: the near wake model and the far wake model. The near wake model includes the blade bounded vortex model and the trailing vortex model. They are both represented by vortex segments as shown in Fig. 3, where the red dots represent the end points of blade segments and the blade dots represent the control points on the segments. The induced velocities of the near wake model are calculated based on the Biot-Savart law.

The velocity induced by the blade bounded vortex model is expressed as

$$V_{ij}^{zb} = \Gamma_j^b \frac{r_i^n \sin\Delta\theta_b \left[r_2(r_j^t - r_i^n\cos\Delta\theta_b) - r_1(r_{j+1}^t - r_i^n\cos\Delta\theta_b)\right]}{4\pi r_1 r_2 \left[r_c^2 + {r_i^n}^2 - (r_i^n\cos\Delta\theta_b)^2\right]} = A_{ij}^b \Gamma_j^b, \tag{1}$$

where the super script b represents the serial number of the blade from 1 to N_b, the sub scripts i and j represent the serial numbers of the control points and the end points of the vortex segments respectively. A_{ij}^b is the influence coefficient determined by the geometry and discretization of the rotor, r_1 and r_2 are the lengths of the vectors from a control point to two end points of blade segments which can be written as

$$r_1 = \sqrt{r_c^2 + {r_i^n}^2 + {r_j^t}^2 - 2r_i^n\cos\Delta\theta_b}, \tag{2}$$

$$r_2 = \sqrt{r_c^2 + {r_i^n}^2 + {r_{j+1}^t}^2 - 2r_i^n\cos\Delta\theta_b}. \tag{3}$$

The trailing vortex model induced velocity at a control point n_i on blade b can be expressed as

$$V_{ij}^{zt} = \Delta\Gamma_j^t \frac{(r_j^t - r_i^n\cos\Delta\theta_b)\left[r_2' r_i^n \sin\Delta\theta_b - r_1(r_j^t - r_i^n\sin\Delta\theta_b)\right]}{4\pi r_1 r_2' \left[r_c^2 + {r_j^t}^2 - 2r_i^n r_j^t\cos\Delta\theta_b - (r_i^n\cos\Delta\theta_b)^2\right]} = A_{ij}^t \Delta\Gamma_j^t, \tag{4}$$

where r_1 and r_2' are the lengths of the vectors from a control point on a blade to the ends of a trailing vortex segment, where r_1 is given in Eq. (2) and r_2' can be defined as

$$r_2' = \sqrt{r_c^2 + {r_i^n}^2 + {r_j^t}^2(1+\theta_1^2) - 2r_i^n r_j^t(\cos\Delta\theta_b + \theta_1 sin\Delta\theta_b)}, \tag{5}$$

and $\Delta\Gamma_j^t$ is the strength of a trailing vortex segment calculated by the difference value of bound vortex strength, namely

$$\Delta\Gamma_j^t = \begin{cases} \Gamma_1^b, & j = 1 \\ \Gamma_j^b - \Gamma_{j-1}^b, & j = 2..N \\ -\Gamma_N^b, & j = N+1 \end{cases}. \tag{6}$$

To keep a low computational cost, the far wake model is represented by the axisymmetric vortex rings, as illustrated in Fig. 4. At given time intervals the vortex rings are released into the wake, with the outer ring shedding from the outboard of the rotor and the inner ring shedding from the inboard of the rotor disc. Each vortex ring acts as independent vortex elements and induces velocity simultaneously in the flow field, on the rotor and on itself.

Assuming a vortex ring with its center marked as O_r and a random field point P, the vector **OP** is given as:

$$\mathbf{OP} = R(\eta, 0, \zeta),\ \eta \in (0, +\infty), \zeta \in (0, +\infty) \tag{7}$$

The analytical solution of a vortex ring with a center O_r induced velocity at a random field point P with $\mathbf{OP} = R(\xi, 0, \zeta)$ is obtained as [20,21].with

$$C_0^2 = 1 + 2\xi + \xi^2 + \zeta^2 + \sigma_c^2, \tag{10}$$

$$C_1^2 = 1 - 2\xi + \xi^2 + \zeta^2 + \sigma_c^2, \tag{11}$$

where V_x is the induced velocity parallel to the ring with the projection of point P on the ring plane lies on the extended line of $\vec{O_r x}$, accordingly, V_z is the induced velocity perpendicular to the ring, Γ is a vortex ring strength, $\sigma_c = r_c/R$ is the non-dimensional vortex core radius, which is taken as 0.0116 considering the self induced velocity [19], and the functions $K(m)$ and $E(m)$ are the first and second type of complete elliptic integrals, respectively, with m defined as:

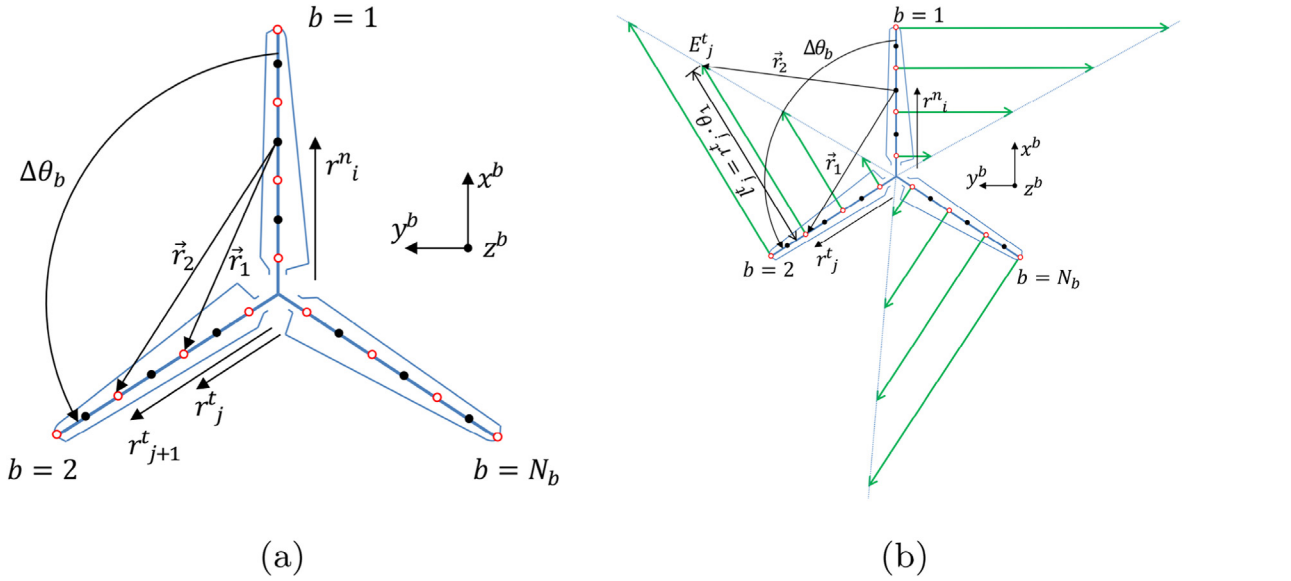

Fig. 3. The blade bound vortex model (a) and the trailed vortex model (b).

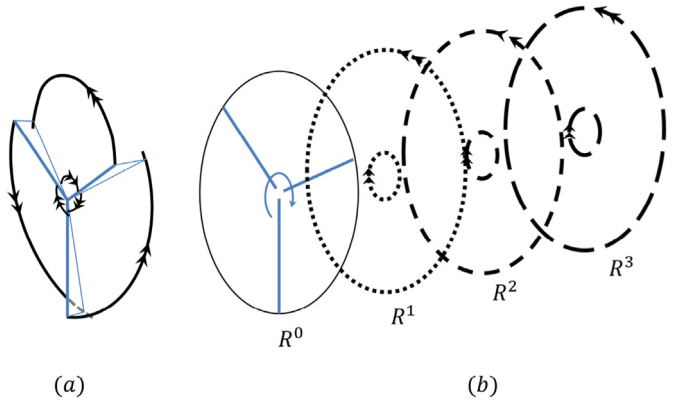

Fig. 4. Schematic representation of a four vortex rings shed by the far wake model.

$$V_x = \frac{\Gamma}{2\pi R C_0}\left[-K(m) + \frac{1+\xi^2+\zeta^2}{C_1^2}E(m)\right]\frac{\zeta}{\xi}, \tag{8}$$

$$V_z = \frac{\Gamma}{2\pi R C_0}\left[K(m) + \frac{1-\xi^2-\zeta^2}{C_1^2}E(m)\right], \tag{9}$$

$$m = \frac{4\xi}{C_0^2}. \tag{12}$$

The vortex rings in the wake change with time, with the motions including the extension or contraction of the diameter, rotation and translation. The parameter set $\mathbf{S}_k$ that describes the position a ring k is written as

$$\mathbf{S}_k = \begin{Bmatrix} x_{O,k} \\ y_{O,k} \\ z_{O,k} \\ R_k \\ \chi_k \\ \beta_k \\ \gamma_k \end{Bmatrix} \quad k = 1, \ldots, N_R, \tag{13}$$

where $\mathbf{O}_k$ is the circle center, R_k is the radius, γ_k, χ_k and β_k are roll, pitch and yaw angles, respectively.

The propagation of vortex ring includes three steps at each time step Δt:

1. Discretize the vortex ring into a number of control points on the radius and calculate the velocities (induced velocity and free stream velocity) at each control point.
2. Calculate the position of the control points with Euler's equation, as

$$\mathbf{S}(t+\Delta t) = \mathbf{S}(t) + \mathbf{V}\Delta t, \tag{14}$$

where V is the speed of a control point in the global coordinate system.

3. Update the position of the vortex ring with all the parameters in $\mathbf{S}_k$ according to the position the control points.

2.2. Blade model

The blade model is built up from the Kutta-Joukowski lift theorem [22] and the blade element theory as shown in Fig. 5, where $\mathbf{F}_l$ is lift force, with the subscripts 1, 2, 3, …distinguish different blade sections.

The Kutta-Joukowski lift theorem defines the lift force on a vortex segment $d\mathbf{l}$ by the production of the air density ρ, the bound vortex strength Γ^b on the segment, and the relative wind velocity to the blade section $\mathbf{V}_R$, as

$$\mathbf{F}_l = \rho\Gamma^b\mathbf{V}_R \times d\mathbf{l}, \tag{15}$$

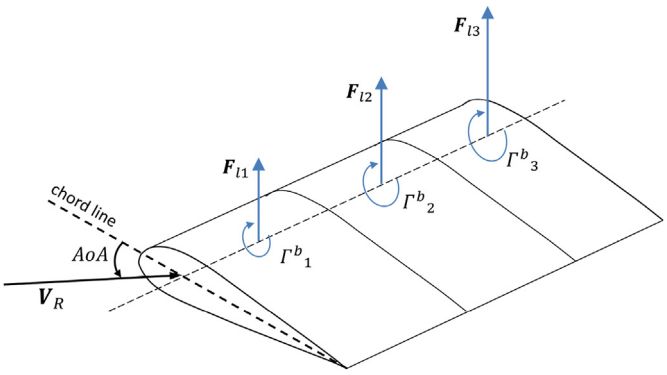

Fig. 5. The blade model of Kutta-Joukowski lift theorem and blade element theory.

The blade element theory calculates the lift force on a blade segment based on the airfoil properties of the segment, which can be expressed as

$$\mathbf{F}_l = \frac{1}{2}\rho \mathbf{V}_R^2 C_l c dl, \tag{16}$$

where c is the chord length, and C_l is the lift coefficient obtained by means of tabulated aerodynamic parameters of the airfoil with a determined angle of attack AoA.

By equating the lift force of Eq. (15) and Eq. (16) on each blade section i, the governing equation set is obtained. For all $N_b \cdot N$ blade sections, a system of $N_b \cdot N$ non-linear equations are obtained and the bound vortex strength Γ^b is solved.

3. NREL 5 MW reference turbine and coordinate systems

The NREL 5 MW reference wind turbine [23] with 5° shaft tilt angle is applied in this paper, with its basic parameters shown in Table 1. The inertial reference coordinate system S marked in red and the rotor-fixed reference coordinate system S' marked in green are shown in Fig. 6.

The inertial reference coordinate system is defined as:

- The origin fixing on the earth.
- x' axis pointing vertically upward opposite to gravity.
- y' axis pointing to the right when looking in the nominal downwind direction.
- z' axis pointing in the nominal (0°) downwind direction.

The rotor-fixed reference coordinate system is defined as:

- The origin fixing on the rotor center, translating and rotating with the tower.
- x'' axis orthogonal with the y'' and z'' axes such that they form a right-handed coordinate system.

Table 1
Characteristics of the NREL 5 MW reference turbine.

Rating	5 MW
Rotor Orientation, Configuration	Upwind, 3 Blades
Rotor, Hub Diameter	126 m, 3 m
Cut-In, Rated, Cut-Out Wind Speed	3 m/s, 11.4 m/s, 25 m/s
Cut-In, Rated Rotor Speed	6.9 rpm, 12.1 rpm
Rated Tip Speed	80 m/s
Overhang, Shaft Tilt, Precone	5 m, 5°, 2.5°
Coordinate Location of Overall CM	(-0.2 m, 0.0 m, 64.0 m)

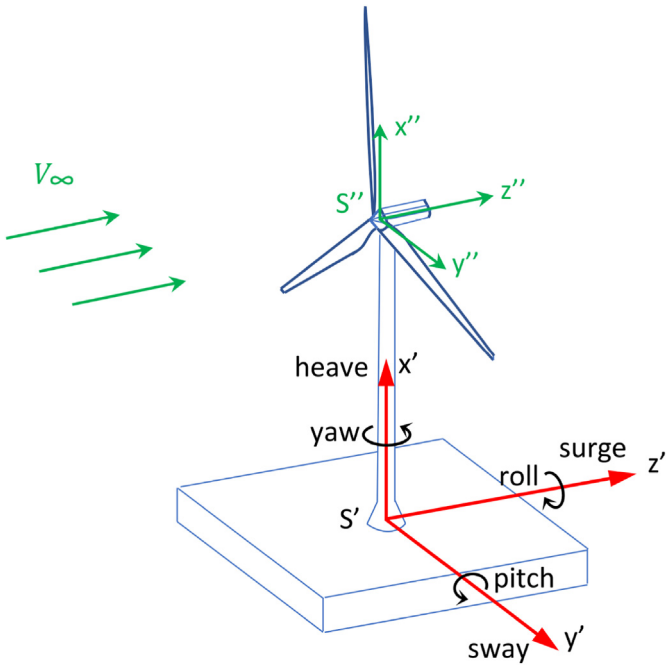

Fig. 6. Inertial reference system and rotor-fixed reference system.

- y'' axis pointing to the right when looking from the tower toward the nominally downwind end of the nacelle.
- z'' axis pointing along the (possibly tilted) shaft in the nominally downwind direction.

In this research, the inertial reference coordinate system is applied when describing the platform motions and the rotor motions, while the rotor-fixed reference coordinate system is applied when describing the flow field around the rotor and the load perceived by the rotor.

4. Criteria for the VRS prediction

Two Criteria are used in this paper to predict the VRS: the axial induction factor 'a' and the Peters' criterion 'p'.

4.1. Criterion 1

The axial induction factor a defined in rotor-fixed reference frame is defined as

$$V_{rel} = (V_\infty - V_p)(1 - a), \tag{17}$$

where V_{rel} is the axial relative velocity to the rotor, V_∞ is the free-stream velocity and V_p is the velocity of the platform motion. The equation Eq. (17) is written in a form which explicitly shows the relationship that when $a = 1$, $V_{rel} = 0$. As shown in Fig. 2, $a = 1$ has several meanings in the diagram. Firstly, the Glauert correction is no longer reliable beyond $a = 1$. Secondly, it is the border line between the turbulent wake state and the propeller brake, with the vortex ring state also occurring around it. Thus, the value $a \geq 1$ is taken as a criteria to identify the occurrence of VRS, and we take it as the center of the VRS rather than the boundary of the VRS.

4.2. Criterion 2

Peters' criterion [14] can be used to predict the VRS of a rotor with both axial and radial velocities which is developed based on

the momentum theory. As shown in Fig. 7, the free stream velocity is defined in the rotor-fixed reference frame, of which the components are given as

$$\frac{\mathbf{a}\cdot\mathbf{b}}{|\mathbf{b}|}=\frac{\mu^2+\eta^2-\nu\eta}{\sqrt{\mu^2+(\nu-\eta)^2}}, \tag{18}$$

where $v_h=|T/2\rho\pi R^2|^{1/2}$, T is the thrust, R is the radius of the rotor; $\eta=(V_\infty-V_p)\sin\alpha/v_h$ is the non-dimensional axial component of free stream velocity; $\nu=\mathbf{V}_I/v_h$ is the non-dimensional induced velocity; and μ is the non-dimensional radial component of the free stream velocity. Accordingly, **a** and **b** are non-dimensional velocity vectors that represent the free stream velocity and wake velocity, respectively.

According to momentum theory, the induced velocity ν inside the stream tube can be replaced by $\kappa\nu$, where the value κ varies from 1.0 at the rotor disc to 2.0 at infinity [13]. Following the same reasoning as before, i.e. the relative velocity should be zero for the VRS boundary, the condition becomes [14].

$$\mu^2=(\kappa\nu-\eta)\left(\eta-\frac{\kappa\nu}{2}\right)=\frac{3}{2}\kappa\nu\eta-\frac{1}{2}\kappa^2\nu^2-\eta^2, \tag{19}$$

combined with the momentum equation which is given in terms of normalized flow-rates [14].

$$\nu^2[\mu^2+(\nu-\eta)^2]=1, \tag{20}$$

the boundary between windmill state and vortex ring state, for the case of $\kappa=1$, is derived as

$$\begin{aligned}\mu^2&=\frac{1}{\nu^2}-\frac{1}{\nu^6},\\ \eta&=\nu-\frac{1}{\nu^3}.\end{aligned} \tag{21}$$

and the vortex ring boundary from vortex ring state to propeller state, for the case of $\kappa=2$, is derived as

$$\begin{aligned}\mu^2&=\frac{1}{\nu^2}-\frac{1}{\nu^6},\\ \eta&=\nu+\frac{1}{\nu^3}.\end{aligned} \tag{22}$$

Considering that the critical values of μ on the propeller side and on the windmill side should be equal, the optimized final criterion is given as

$$\begin{aligned}\mu^2&=\frac{1}{\nu^2}-\frac{1}{\nu^6},\\ \eta&=\nu\pm\frac{1}{\nu^3},\\ \lambda&=\nu-\eta=\mp\frac{1}{\nu^3}.\end{aligned} \tag{23}$$

Fig. 8 shows the results of Equation (23), where the vortex ring state occurs inside the axisymmetric curve in $\mu-\lambda$ plane. The upper half of the curve represents the border with the windmill state and the lower half of the curve represents the border with the propeller state.

5. Load cases description

To facilitate the comparison with the literature [10], the same load cases and the same rotor with prescribed rotational speeds are simulated in the paper. As summarized in Table 2, the rotor with prescribed surge motions was investigated under a below-rated wind speed of 7 m/s and the rated wind speed of 11.4 m/s and the bottom-fixed rotor operating with the same wind speeds was taken as a reference. The purpose of this set of load case design in the literature was to capture the vortex ring state and propeller state with surge motion of the rotor. To this end, the maximum surge velocity of the moving rotor was designed to be larger than the relative wind speed for the below-rated load case (as shown in Table 2 of Kyle et al. [10]).

In Table 2, the load cases are labeled as: RF, RS, BF and BS, where 'R' represents 'Rated' wind speed, 'B' represents 'Below' rated wind speed, 'F' represents 'Fixed' and 'S' represents 'Surge'. V_∞ is the free stream velocity and A_s is the amplitude of the sinusoidal surge motion. Accordingly, the surge displacement, χ_s, is defined as:

$$\chi_s=A_s\sin(\omega_s t), \tag{24}$$

where ω_s is the surge frequency in rad/s and t is time in seconds. And the surge velocity of the rotor is identified as:

$$u_s=\frac{d\chi_s}{dt}=A_s\omega_s\cos(\omega_s t). \tag{25}$$

The original design of this set of load cases is formulated according to the response amplitude operators (RAO) which predicts the surge motion of the whole wind system, with the assumption

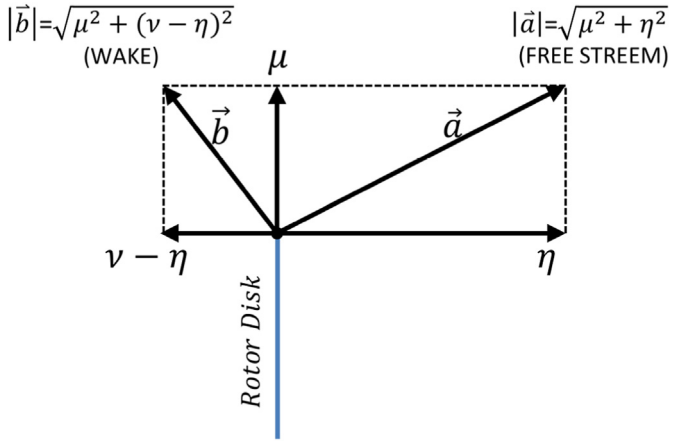

Fig. 7. The velocity components of Peters' criterion.

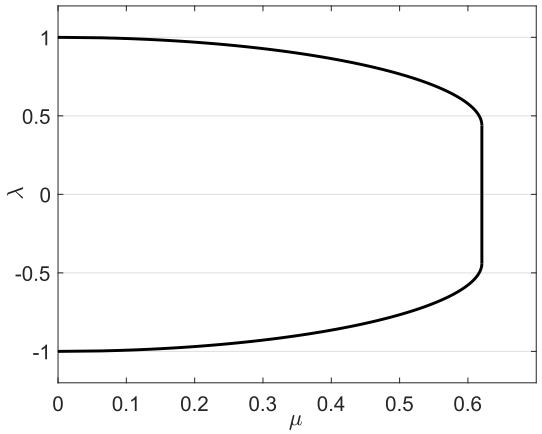

Fig. 8. The boundaries of Peters' criterion in $\mu-\lambda$ plane.

Table 2
Rated and below-rated load cases.

Lable	Rotation rate [rpm]	V_∞ [m/s]	A_s [m]	Surge period [s]
RF	12.10	11.4	–	–
RS	12.10	11.4	9.4	8.1
BF	8.47	7.0	–	–
BS	8.47	7.0	9.4	8.1

that the 5 MW NREL reference wind turbine is mounted on a barge platform. The translational RAO is defined as [10]:

$$RAO_i(\omega) = \frac{\Xi_i(\omega)}{A_{wave}} \; i = 1, 2, 3. \tag{26}$$

where ω is the wave frequency, Ξ is the system response amplitude, A_{wave} is the wave amplitude, and $i = 1, 2, 3$ corresponding to surge, heave and sway, respectively. The barge surge RAO amplitude is taken as 5. In order to get the VRS from a pure surge motion of the platform, the wave condition selection is: wave height $A_{wave} = 1.87m$ and wave period of $T = 8.1s$, which leads to a platform surge amplitude of 9.4m and surge period of 8.1s. The surge frequency is quite high, which leads to only a short period during the surge cycle for the onset and development of VRS (approximately 2s as mentioned in the literature [10]).

It is worth mentioning that according to our previous research results [4], the 5 MW NREL reference wind turbine mounted on a barge platform is indeed very sensitive to the wave loads, and the VRS is more likely to occur than with spar or tension-leg platform under the same wind and wave conditions. In this research, we will use the same load cases of Kyle's model to facilitate the comparison. However, we found that the VRS may also occur to FOWTs in much milder surge motions of the platform (lower amplitude and lower frequency) than the load cases we analysis here, which is mainly because the pitch motion also plays an important role in the VRS.

Each load case was simulated for 150 s, and the data is taken into account after 50s when the wake structure is developed sufficiently. According to the rotation rate of the rotor, the time step Δt for 'RF' and 'RS' is 0.1377s and for 'BF' and 'BS' is 0.1968s.

The literature use a finite volume discretization of the incompressible Reynolds-Averaged Navier-Stokes equations in OpenFOAM. In this work, the free-wake vortex model as presented above is used. In addition, the way in which the occurrence of the VRS is identified in this paper is different from the literature, which is explained in detail in Section 6.

6. Research methods comparison with the literature

Considering that the research about the VRS of FOWTs is still in a very early stage, the concept of the VRS is not extensively acquainted by the academic community, firstly we compare the basic concepts of the VRS of FOWTs, computational methods and identification methods of VRS we adopted with the ones used in Kyle's model [10] as summarized in Table 3.

Through the comparison, it is seen that we are on the same track with the literature in respect of the description of the VRS of FOWTs. However, we adopt different computational methods for the rotor aerodynamic simulation, and different ways of identifying the occurrence of the VRS.

7. Comparing the VRS prediction results with Kyle's model

7.1. C_T and angle of attack

In order to guarantee the reliability of the comparison of the VRS results, we first compared the aerodynamic parameters thrust coefficient C_T and angle of attack with the literature. The thrust coefficient C_T is defined as

$$C_T = \frac{T_x}{0.5\rho_{air}A_{rotor}V_\infty}, \tag{27}$$

where T_x in the force normal to the rotor, ρ_{air} is the air density, A_{rotor} is the rotor swept area and V_∞ is the free stream velocity.

Firstly, the C_T for fixed rotors (RF and BF) are compared with that of Kyle's model and the output of FAST v8 [4,24], as shown in Fig. 9 and Fig. 10. The figures show that at both rated wind speed (RF) and below rated wind speed (BF), the C_T from the vortex method fluctuate closely around the output of FAST. The fluctuation is due to the periodical release of vortex rings into the wake of the numerical method. Also, the results from Kyle's CFD model is slightly higher than the value obtained by FAST and the vortex method. Since the CFD model presents the initial 30 s' result of the simulation (with the first 9 s results omitted [10]), the wake is not fully developed at that moment and the induced velocity can be lower than normal. While the results from the vortex method and FAST are obtained when the simulations are stable. Accordingly, all the results presented in the figures are considered to be reasonable.

Fig. 11 and Fig. 12 show a comparison of C_T between the present method and Kyle's method [10] for the rotor with prescribed surge motions. From the figures it can be seen that the two C_T curves match well with each other. In general, the two curves fluctuate with the same periods (the phases are also adjusted to be the same to facilitate the comparison), and their average values and the amplitudes of the fluctuation are also the same with each other. For the load case 'BS', negative values of C_T are apparent at the bottom of the curves, while for the load case 'RS', only positive values are obtained. In addition, the curves from the present vortex method are flat at the top of the curves and are sharp at the lower part of the curves, which is also the same with the literature. The fluctuation at the top of the curves from the CFD model is explained as an unsteady aerodynamic phenomenon during windmill state of the rotor [10]. Despite of this difference, the results from both methods are considered to be comparable and in good agreement.

The angle of attacks (AoA) are also compared with the literature for the four load cases: RF, RS, BF and BS, as shown in Fig. 13 and Fig. 14. In the figures, the AoA curves of 'Present - RF' and 'Present - BF' are the average AoAs of the fixed rotor, which are compared with the AoA curves of 'Kyle - RF' and 'Kyle - BF' respectively, and the results are match well with each other. The AoA curves of 'Present high - RS', 'Present high - BS' are the AoAs with the same value of C_T (at 16 s of simulation time) of Kyle's model and they are compared with the AoAs of 'Kyle - RS' and 'Kyle - BS' respectively, and the results are match well with each other. In these figures, we also output the AoAs when the C_T reach the lowest point, which are marked as 'Present low - FS' and 'Present low - BS'. It can be seen that they are all negative values. Taking the negative twist angle 'Blade twist' as a reference it is found that the AoAs of 'Present low - RS' are higher than the negative twist angles. Thus, the lowest C_T is above zero as shown in Fig. 11. By contrast, the AoAs of 'Present low - BS' are lower than the negative twist angles along the span, which explains the reason why the lowest C_T is negative as shown in Fig. 12.

7.2. Comparative analysis of the VRS prediction results

In helicopter's realm, different criteria for the VRS prediction are developed based on momentum theory, field test, experiments, numerical simulation and so on. Different criteria can give different prediction results of the VRS [11]. In our previous study, some VRS

Table 3
Research methods comparison with Kyle's model [10].

1. The description of the VRS Kyle The vortices in the wake recirculate around the rotor resulting in flow detachment and a reduction in lift. Dong The same.
2. The causation of the VRS of FOWTs Kyle When the rotor moves downwind at a speed similar to the wake it produced. Dong The same.
3. The computational methodology Kyle Finite volume CFD method in OpenFOAM is used to solve the incompressible Reynolds-Averaged Navier-Stokes equations. Dong Free wake vortex ring method is used based on the potential flow theory.
4. The identification of VRS Kyle Firstly the propeller state is identified when the relative velocity at the rotor decreasing to and surpassing zero, and then, the VRS is identified during the propeller state event when the blade vortex interaction at the tip and strong flow recirculation at the root are visible. Dong Two criteria are used to predict the VRS: the axial induction factor $a \geq 1$ and the Peters' criterion.

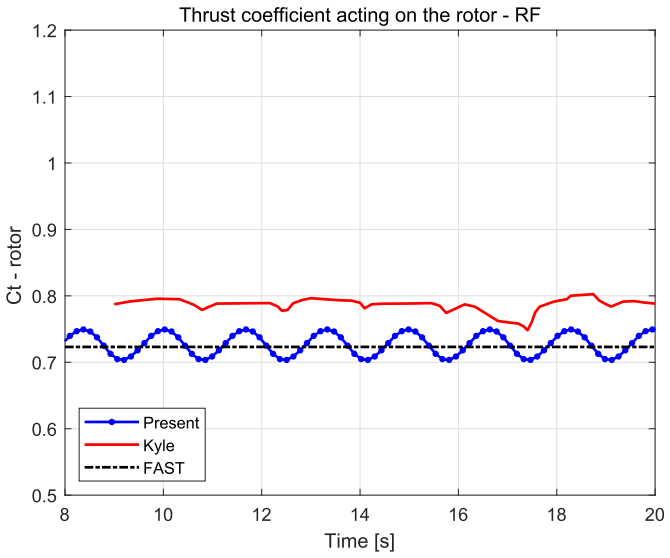

Fig. 9. Thrust coefficient acting on fixed rotor (RF).

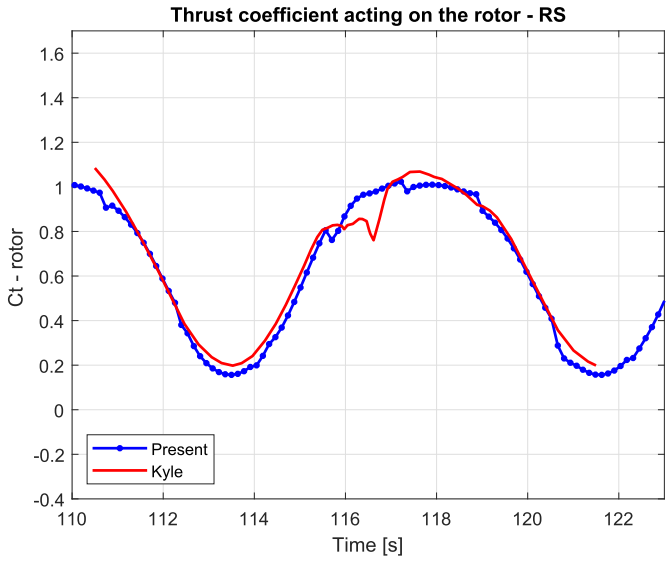

Fig. 11. Thrust coefficient acting on fixed rotor (RS).

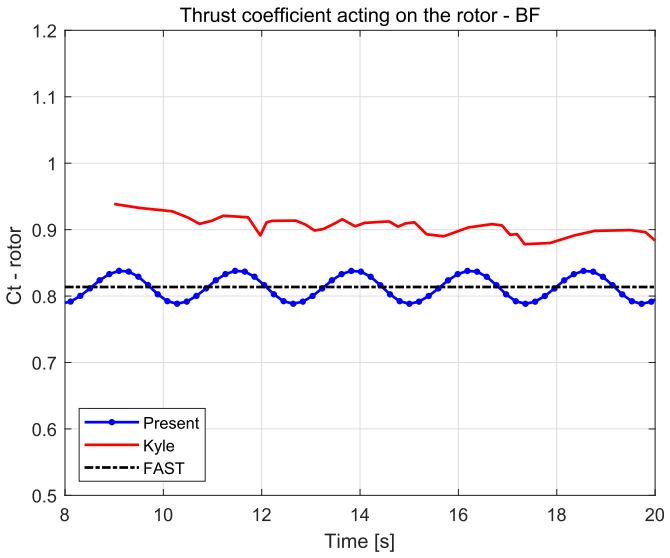

Fig. 10. Thrust coefficient acting on fixed rotor (BF).

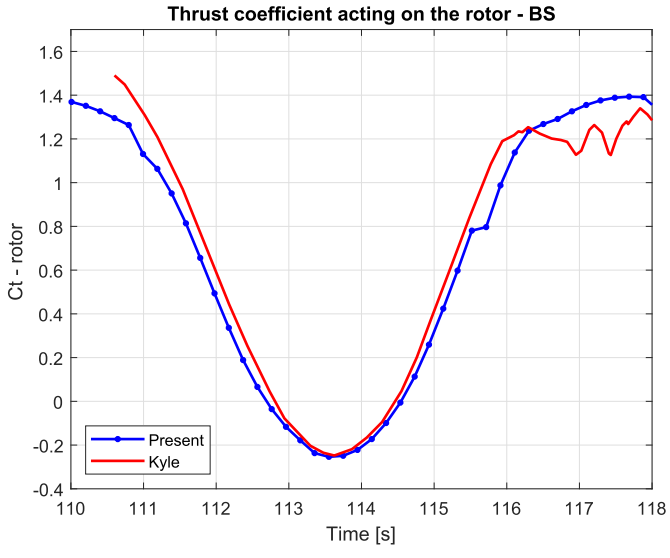

Fig. 12. Thrust coefficient acting on fixed rotor (BS).

prediction criteria were introduced from helicopter's realm and applied to FOWTs [4]. In this paper, the axial induction factor $a = 1$ and Peters' criterion are selected for the VRS prediction and the results are further verified by comparing to a CFD model.

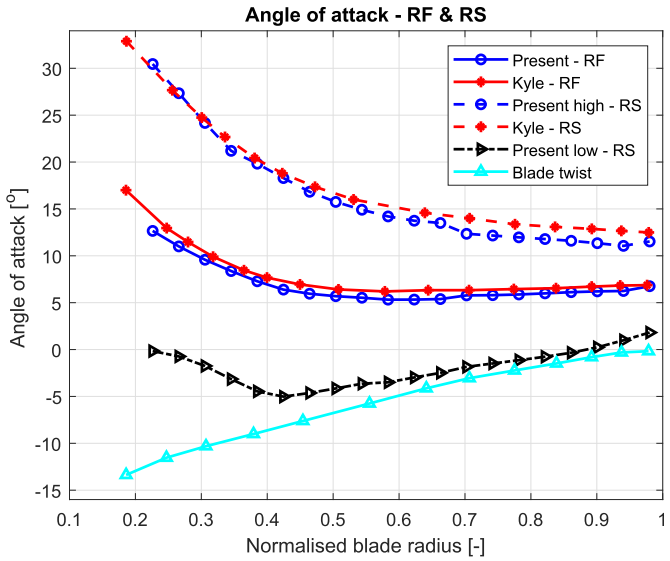

Fig. 13. Angle of attack acting on the airfoils of the blade (11.4 m/s).

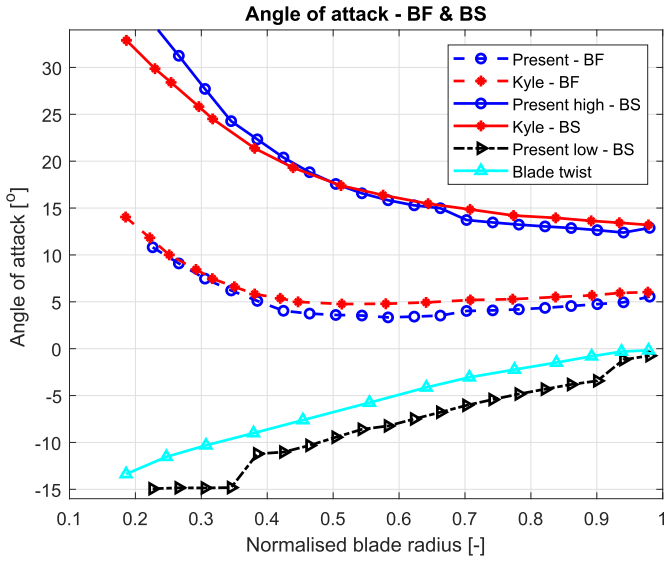

Fig. 14. Angle of attack acting on the airfoils of the blade (7 m/s).

7.2.1. *The VRS prediction results from two criteria*

The VRS boundaries are predicted for the FOWT under surge motions. The results of the load cases 'RS' and 'BS' according to the axial induction factor 'a' and the Peters' criterion 'p' respectively are shown from Fig. 15 to Fig. 18. The figures are plotted based on the results of one of the three blades of the rotor, where V_n is the relative wind speed normal to the rotor taken from the middle of the blade and 'surge' is the surge displacement at the rotor center. The horizontal axis represents the simulation time and the vertical axis represents the blade span. Figs. 15 and 16 show the VRS prediction results for 'RS'. In Fig. 15 the purple area indicates $0.5 \leq a < 1$ and the yellow area indicates $a \geq 1$. Fig. 16 the green strips remark the occurrence of the VRS. As expected, the $a \geq 1$ criterion predicted narrower areas of the VRS than that predicted with 'p'.

Similarly, Figs. 17 and 18 show the VRS prediction results for 'BS'. The VRS areas occur periodically with the rotor motion, which are corresponding to the time periods in which V_n is relatively low and the rotor is moving downwind with surge motion. It is also found that the VRS area is very small at the tip of the blade where the relative wind velocity is large, which is also seen in Kyle's analysis for 'BS'. As was found in the previous analysis, the VRS areas predicted with 'a' are smaller than those predicted with 'p'.

The prediction results show that the VRS rate of 'BS' is significantly higher than that of 'RS'. In Fig. 18 there are some yellow islands inside the green strips, which indicates that the velocity components pass through the lower boundary of Peters' criterion as shown in Fig. 8 and go into the propeller state for the 'BS' case. By contrast, there is no yellow islands appear in Fig. 16, which means that there is no propeller state occur for the 'RS' case.

7.2.2. *The VRS prediction results*

For the 'RS' case, in the literature, no flow reversal was observed, thus the propeller state does not occur and the VRS was not analyzed. In our research, similar conclusions can be made for the propeller state. According to 'a', as is observed in Fig. 15, only minor areas of $a \geq 1$ is obtained, which indicates that the flow reversal occurs only in local areas with very short time durations. In addition, according to 'p' as shown in Fig. 16, the propeller state is also not predicted. However, Fig. 16 shows that the VRS is significantly predicted, which means that Peters' criterion predicts the occurrence of the VRS before the mean thrust becomes negative.

For the 'BS' case, in the literature, flow reversal was observed, thus the propeller state was firstly identified and then the VRS was further analyzed during the propeller state even. The VRS was identified when the blade vortex interaction at the tip and flow recirculation at the root were visible. In our research, the propeller state is also captured according to 'p' as analyzed before. Fig. 18 indicates that the rotor experienced the working state change from the windmill state to vortex ring state and then to propeller state. Thus, both of the VRS and the propeller state are captured by us and the literature.

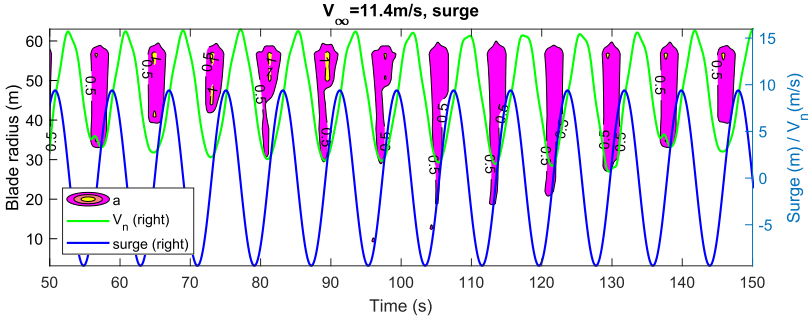

Fig. 15. Regions of VRS predicted with 'a' (in yellow) for 'RS'.

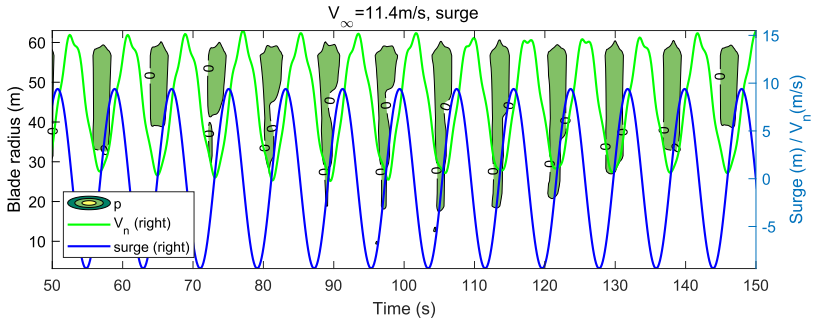

Fig. 16. Regions of VRS predicted with 'p' (in green) for 'RS'.

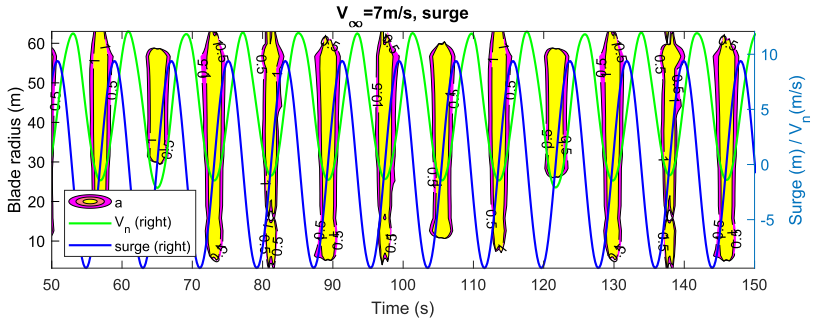

Fig. 17. Regions of VRS predicted with 'a' (in yellow) for 'BS'.

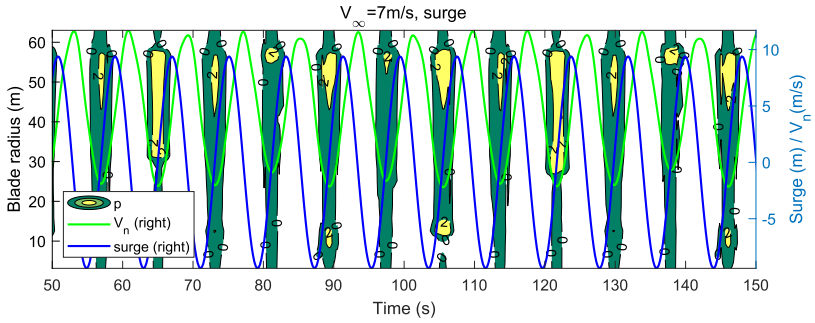

Fig. 18. Regions of VRS predicted with 'p' (in green) for 'BS'.

7.2.3. The location and time range of the VRS

The location and time range of the VRS are further compared with the literature. In regard to the location, the research agrees with the literature that both the VRS and the propeller state are developed around the centers corresponding to the downwind peak velocities of the rotor in each cycle of the platform motion. However, in the literature, the propeller state is identified when the relative velocity at the rotor decreasing to and surpassing zero, which can also be indicated by negative angles of attack or thrust coefficients. In addition, it seems that the VRS is defined after the occurrence of the propeller state, when a zero or negative relative velocity is maintained so that the tip and root vortices cannot propagate downstream. In our research, the location of the VRS is found between the windmill state and the propeller state according to Peters' prediction criterion, which is a main difference from Kyle's model but consistent with the illustration in Fig. 2.

As for the time range, in the literature, the propeller state captured in 'BS' case lasts for about 1.5–2 s during each cycle of the rotor motion and the VRS also occurs within this period of time. By contrast, in our research, the statistic data of 150s simulation show that the ratio for the occurrence of the VRS is found to be 27%, and the average period is $8.1s \times 27\% = 2.2s$ according to 'a'. According to 'p', the ratio for the occurrence of the VRS and the propeller state together in time series is 42% and the average period is 3.4*s*, while the ratio for the propeller state alone is 20% and the average period is 1.62*s*. Thus, the time range of the propeller state from the two studies are consistent with each other, which is mainly because the flow reversal moments calculated with both the CFD method and the vortex method are the same. However, the time ranges of the VRS from our research are significantly larger according to both of the criteria 'a' and 'p', which is mainly because we captured the VRS outside of the propeller state even rather than inside.

8. Conclusion

In this paper, the vortex ring state and propeller state of a floating offshore wind turbine are simulated and predicted with a free wake vortex method, and the results are compared with those

from a CFD model. Firstly, the aerodynamic parameters including thrust coefficients and the angle of attack are compared with a CFD method and a BEM method with convincing results. Secondly, the vortex ring state and propeller state boundaries are predicted with the axial induction factor and the Peters' criterion for the rotor with surge motions. And then, we compared both the research methods and the prediction results of the two working state with the CFD model. Through the comparison results, qualitatively, the Peters' criterion is verified to be successful in terms of predicting the occurrence of both the vortex ring state and propeller state. The location and duration of the propeller state are found to be consistent with the literature. However, the location and duration of the vortex ring state identified in this research are significantly different from the CFD model. We consider that the vortex ring state occurs between the windmill state and the propeller state, rather than within the propeller event.

This paper paves the road for further research about the working states of FOWTs. It is worth mentioning that the axial induction factor and the Peters' criterion are not the only methods for the prediction of the working states. There are many different criteria that worth research on. Future work will focus on the influence of different working states on the performance of FOWTs, in particular, possible mitigation measures.

CRediT authorship contribution statement

Jing Dong: Conceptualization, Methodology, Software, Validation, Formal analysis, Investigation, Resources, Data curation, Writing – original draft, Writing – review & editing, Visualization, Project administration, Funding acquisition. **Axelle Viré:** Writing – review & editing, Project administration. **Zhangrui Li:** Software, Investigation, Resources, Writing – review & editing.

Declaration of competing interest

The authors declare that they have no known competing financial interests or personal relationships that could have appeared to influence the work reported in this paper.

Acknowledgements

Dong would like to acknowledge support from China Scholarship Council. We would like to thank professor Simon Watson in TU Delft for his support of this work. Many thanks are also extended to Jacobus B. de Vaal of the Institute for Energy Technology in Norway for his generous assistance for the development of the vortex code. We would also like to express our sincere gratitude to Ryan Kyle for explaining his research to us.

References

[1] D. Eggleston, F. Stoddard, Wind Turbine Engineering Design, Van Nostrand Reinhold Company, New York, 1987.
[2] J. Leishman, Principles of Helicopter Aerodynamics, Cambridge University Press, Cambridge, 2006.
[3] D.J. Varnes, Development of a Helicopter Vortex Ring State Warning System through a Moving Map Display Computer, Calhoun, 1999. https://calhoun.nps.edu/handle/10945/26475.
[4] J. Dong, A. Viré, Comparative analysis of different criteria for the prediction of vortex ring state of floating offshore wind turbines, Renew. Energy 163 (2021) 882–909, https://doi.org/10.1016/j.renene.2020.08.027.
[5] T. Sebastian, M. Lackner, Characterization of the unsteady aerodynamics of offshore floating wind turbines, Wind Energy 16 (3) (2013) 339–352, https://doi.org/10.1002/we.545.
[6] T. Tran, D. Kim, The platform pitching motion of floating offshore wind turbine: a preliminary unsteady aerodynamic analysis, J. Wind Eng. Ind. Aerod. 142 (C9) (2015) 65–81, https://doi.org/10.1016/j.jweia.2015.03.009.
[7] T. Tran, D. Kim, J. Song, Computational fluid dynamic analysis of a floating offshore wind turbine experiencing platform pitching motion, Energies 7 (8) (2014) 5011–5026, https://doi.org/10.3390/en7085011.
[8] M. Jeon, S. Lee, S. Lee, Unsteady aerodynamics of offshore floating wind turbines in platform pitching motion using vortex lattice method, Renew. Energy 65 (2–3) (2014) 207–212, https://doi.org/10.1016/j.renene.2013.09.009.
[9] R. Kyle, Alleviation of the Vortex-Ring State for Floating Offshore Wind Turbines Using a Modified Blade-Tip Shape, ETP Conference, Wind session, 2017.
[10] R. Kyle, Y.C. Lee, W.-G. Früh, Propeller and vortex ring state for floating offshore wind turbines during surge, Renew. Energy 155 (2020) 645–657, https://doi.org/10.1016/j.renene.2020.03.105. http://www.sciencedirect.com/science/article/pii/S0960148120304377.
[11] P. Basset, C. Chen, J.R. Prasad, S. Kolb, Prediction of vortex ring state boundary of a helicopter in descending flight by simulation, J. Am. Helicopter Soc. 53 (2008) 139–151, https://doi.org/10.4050/JAHS.53.139.
[12] J. Dong, A. Viré, Predicting the occurrence of the vortex ring state for floating offshore wind turbines, J. Phys. Conf. 1618 (2020), https://doi.org/10.1088/1742-6596/1618/5/052044.
[13] J. Wolkovitch, Analytical prediction of vortex-ring boundaries for helicopter in steep descents, J. Am. Helicopter Soc. 17 (1972) 13–19, https://doi.org/10.4050/JAHS.17.13.
[14] D. Peters, S. Chen, Momentum theory, dynamic inflow, and the vortex-ring state, J. Am. Helicopter Soc. 27 (3) (1982) 18–24, https://doi.org/10.4050/JAHS.27.18.
[15] T. Sebastian, M. Lackner, Analysis of the induction and wake evolution of an offshore floating wind turbine, Energies 5 (2012) 968–1000, https://doi.org/10.3390/en5040968.
[16] H. Lee, D.-J. Lee, Effects of platform motions on aerodynamic performance and unsteady wake evolution of a floating offshore wind turbine, Renew. Energy 143 (2019) 9–23, https://doi.org/10.1016/j.renene.2019.04.134. http://www.sciencedirect.com/science/article/pii/S0960148119306184.
[17] A. Afjeh, Wake Effects on the Aerodynamic Performance of Horizontal axis Wind Turbines, Tech. rep, NASA contractor report, 1984, 09.
[18] J. de Vaal, M. Hansen, T. Moan, Influence of rigid body motions on rotor induced velocities and aerodynamic loads of a floating horizontal axis wind turbine, in: ASME. International Conference on Offshore Mechanics and Arctic Engineering 9B, Ocean Renewable Energy, 2014, https://doi.org/10.1115/OMAE2014-24227.
[19] J. Dong, A. Viré, C. Ferreira, Z. Li, G. Van Bussel, A modified free wake vortex ring method for horizontal-axiswind turbines, Energies 12 (20) (2019) 10, https://doi.org/10.3390/en12203900.
[20] S. Newman, The Induced Velocity of a Vortex Ring Filament, AFM Technical Reports 11/03, University of Southampton, School of Engineering Sciences, 2011.
[21] S. Yoon, S. Heister, Analytical formulas for the velocity field induced by an infinitely thin vortex ring, Int. J. Numer. Methods Fluid. 44 (2004) 665–672, https://doi.org/10.1002/fld.666.
[22] D. Phillips, W.F. Snyder, Modern adaptation of Prandtl's classic lifting-line theory, J. Aircraft 34 (4) (2000) 622–670, https://doi.org/10.2514/2.2649.
[23] J. Jonkman, S. Butterfield, W. Musial, G. Scott, Definition of a 5-mw Reference Wind Turbine for Offshore System Development, Tech. rep, NREL, 2009.
[24] B. Jonkman, J. Jonkman, Fast v8.15.00a-Bjj, Tech. rep, NREL, 2016.